

# Determination of Non-Universal Supergravity Models at the Large Hadron Collider

Bhaskar Dutta<sup>1</sup>, Teruki Kamon<sup>1,2,3</sup>, Abram Krislock<sup>1</sup>, Nikolay Kolev<sup>4</sup>,  
Youngdo Oh<sup>3</sup>

<sup>1</sup> *Department of Physics, Texas A&M University, College Station, TX 77843-4242, USA*

<sup>2</sup> *Fermi National Accelerator Laboratory, Batavia, Illinois 60510, USA*

<sup>3</sup> *Department of Physics, Kyungpook National University, Daegu 702-701, South Korea*

<sup>4</sup> *Department of Physics, University of Regina, Regina, SK S4S 0A2, Canada*

## Abstract

We examine a well motivated non-universal supergravity model where the Higgs boson masses are not unified with the other scalars at the grand unified scale at the LHC. The dark matter content can easily be satisfied in this model by having a larger Higgsino component in the lightest neutralino. Typical final states in such a scenario at the LHC involve  $W$  bosons. We develop a bi-event subtraction technique to remove a huge combinatorial background to identify  $W \rightarrow jj$  decays. This is also a key technique to reconstruct supersymmetric particle masses in order to determine the model parameters. With the model parameters, we find that the dark matter content of the universe can be determined in agreement with existing experimental results.

# 1 Introduction

The dark matter content of the universe today has been measured very precisely by the WMAP experiment [1] which shows that the energy density of the universe is comprised of 23% dark matter. Supersymmetry (SUSY) models with conservation of R-parity can naturally explain the dark matter content, as well as solving many problems inherent in the Standard Model (SM). In most SUSY models, the weakly interacting lightest neutralino is an excellent dark matter candidate [2] since the dark matter content of the universe can be satisfied in these SUSY models.

The existence of this dark matter connection is under tremendous experimental investigation at the Large Hadron Collider (LHC) and at direct and indirect dark matter detection experiments. At the LHC, the dark matter hypothesis can be tested by producing the dark matter particles which will give rise to missing energy signal. In addition to the dark matter candidate, other SUSY particles will also be produced. Attempts will be made to measure SUSY particle masses and model parameters which will be used to estimate the dark matter content based on the available measurements at the LHC. It will be very interesting if such an estimate of the dark matter relic density is close to the measurement of WMAP [1] because we will be on the verge of establishing a true connection between particle physics and cosmology. Of course, the measurements from the direct and indirect detection experiments need to support this connection as well.

The Minimal Supersymmetric Standard Model (MSSM) is a very general supersymmetric extension of the SM which has more than a hundred parameters to specify the model. It would be impossible to completely reconstruct this entire model at the LHC since that would require finding more than a hundred measurable quantities to determine the model parameters. Extraction of the measurable quantities, end points, and peak positions of different distributions is not easy due to severe background problems from the model itself. In such a situation, our approach is to use well motivated SUSY models with fewer parameters to study and understand the final states and associated observables. This way, we can determine all the model parameters and calculate the dark matter content. Also, the techniques we develop to extract the measurable quantities can also be applied to models with larger sets of parameters.

We first used the minimal supergravity motivated model (mSUGRA) [3]. The mSUGRA model has the feature that many SUSY masses unify at the grand unified scale (GUT scale). This feature makes the model very simple, requiring only four parameters and a sign to determine all of the SUSY particle spectrum. The choice of the sign can be motivated by the branching ratio,  $\mathcal{B}(b \rightarrow s\gamma)$  [4]. Thus to reconstruct this model at the LHC requires only four distinct measurements.

In previous studies [5, 6, 7, 8], we have developed methods of measuring mSUGRA at the LHC. We found that the dark matter content can be measured with an accuracy comparable to the WMAP measurement. We also found that different dark matter allowed regions have different smoking gun signals at the LHC in the mSUGRA model.

Having all scalar masses unified at the GUT scale is perhaps too simple an assumption. On the other hand, determining many parameters at the LHC is also a very difficult task. This study takes the first step in a more general direction. We study a non-universal supergravity (nuSUGRA) model, where the Higgs masses no longer unify at the GUT scale with the other

scalar SUSY particles. This Higgs sector non-universality is easily imagined because it is a completely different sector of matter from the SUSY partners of the quarks and leptons. This type of model has been studied extensively in the context of dark matter [9, 10].

This nuSUGRA model has six parameters instead of four, with two new parameters for the two Higgs doublet masses. The difficulty in any of these studies is to have enough experimentally measurable observables to determine all of the model parameters. In this work, we investigate the decay chains and final states of the model to identify typical signals and to find these observables. This task is well worth the effort even if this nuSUGRA model is not true, since the measurement techniques we uncover can be applied to any other model with similar signals to measure relations between SUSY particle masses.

The SUSY measurements at the LHC involve cascade decays arising from the colored SUSY particles, the squarks and gluinos. SUSY models with R-parity are difficult to measure, since each event has its own background. This is because R-parity demands that SUSY particles always be produced in pairs. Thus, each event has two SUSY decay chains which can be a background to each other. In this paper, we demonstrate a technique to isolate only the decay chain we want to look at by effectively subtracting out the signal from the other chain. This technique is a method which eliminates a large amount of background from the signal we want to measure.

This technique combines with other measurement techniques to make enough measurements to fully reconstruct all the model parameters. We then use those parameters to determine the entire SUSY spectrum, as well as to determine the dark matter relic density of the universe.

The outline of this paper is as follows. In section 2, we describe in more detail the nature of the nuSUGRA model. In section 3, we describe the signals that would be seen from this model at the LHC, as well as the observables and measurement techniques needed to fully determine this model. In section 4, we compile all the measurement results together to determine the model parameters and estimate their uncertainty. We conclude in section 5.

## 2 nuSUGRA Model and Benchmark Point

We first review the mSUGRA model in order to describe the nuSUGRA model. The mSUGRA model has the attractive feature that many of the SUSY particle masses are unified at the GUT scale. Thus, it needs only four parameters and a sign to specify the entire model. These parameters are:

- The unified scalar mass at the GUT scale,  $m_0$ ,
- The unified gaugino mass at the GUT scale,  $m_{1/2}$ ,
- The trilinear coupling at the GUT scale,  $A_0$ ,
- The ratio of the vacuum expectation values of the two Higgs doublets,  $\tan \beta$ , and
- The sign of the Higgs bilinear coupling,  $\text{sign}(\mu)$ .

Since these model parameters (along with the SM parameters) specify all of the masses and mixings for the SUSY particles in the model, they also determine whether or not this model

predicts the correct amount of dark matter left in the universe today. If we assume a history of the universe where the dark matter particles, the neutralinos, were in thermal equilibrium in the universe at early times, then a large region of the mSUGRA parameter space actually predicts too much dark matter today. This is due to the neutralinos not being able to annihilate enough in the early universe. However, certain regions of mSUGRA parameter space allow for mechanisms where the neutralino annihilation cross-section is large enough during early times which lead to the correct amount of dark matter today [11].

For instance, the co-annihilation region has the characteristic feature that the stau particle has a mass very close to that of the neutralino. This allows for the neutralino to co-annihilate with the lightest stau particle in the early universe. This extra annihilation mechanism increases the total annihilation cross-section for the neutralino [12]. It is also possible to have stop coannihilation if  $A_0$  has a large yet negative value [13]. Another region, called the  $A$ -funnel region, has the feature that the neutralino mass is very close to being half the mass of the pseudo-scalar Higgs boson ( $A^0$ ). Thus, there is a resonance when the neutralinos annihilate through this  $A^0$  channel, which increases the annihilation cross-section [14]. Light Higgs resonance annihilation is also possible for small values of  $m_{1/2}$  [15].

A third region, called the focus point/hyperbolic branch region, has a “focused” value for the parameter  $\mu$  [16]. This parameter is determined in mSUGRA by the electroweak symmetry breaking requirement. In the focus point region, this requirement causes the value of  $\mu$  to be very small. The small value of  $\mu$  causes the lightest neutralino to be very Higgs-like and couple strongly to heavier particles. Thus, neutralino annihilation diagrams containing  $Z$  or Higgs bosons are favored. This effect causes the annihilation cross-section to be large enough to have the right amount of dark matter today.

There is another way to achieve this small value for the  $\mu$  parameter: The nuSUGRA model. In the nuSUGRA model, the Higgs bosons are given a non-universal mass. Normally, for the mSUGRA model, the Higgs bosons, being scalar particles, have a mass of  $m_0$  at the GUT scale. Since the Higgs masses are intimately related to the electroweak symmetry breaking condition, adjusting the Higgs masses has a direct effect on the value of  $\mu$ . In a sense, we are promoting  $\mu$  to a free parameter, since for any particular choice of the other four parameters, we can adjust  $\mu$  by adjusting Higgs masses.

Since there are two Higgs doublets in SUSY models, we can have a parameter for each of their masses at the GUT scale, i.e.,  $m_{H_u}^2 = (1 + \delta_{H_u})m_0^2$ ,  $m_{H_d}^2 = (1 + \delta_{H_d})m_0^2$ . However, only one of the Higgs masses affects the value of  $\mu$ . The value of  $\mu^2$  at the electroweak scale in terms of the GUT scale parameters is determined by the renormalization group equations (RGEs). In general, one must solve these numerically. However, one can get a qualitative understanding of the effects of the  $\delta_H$ ’s from an analytic solution which is valid for low and intermediate  $\tan \beta$  [9]:

$$\mu^2 = \frac{t^2}{t^2 - 1} \left[ \left( \frac{1 - 3D_0}{2} - \frac{1}{t^2} \right) + \left( -\frac{1 + D_0}{2} \delta_{H_u} + \frac{\delta_{H_d}}{t^2} \right) \right] m_0^2 + \Delta, \quad (1)$$

where  $t \equiv \tan \beta$ ,  $D_0 \simeq 1 - (m_t/200\sin \beta)^2$ , and  $\Delta$  contains the universal parts (which are independent of the  $\delta_H$ ’s) and loop corrections. In general  $D_0$  is small ( $D_0 \leq 0.23$ ). Equation 1 shows that  $\mu$  is primarily sensitive to  $\delta_{H_u}$ . However, the pseudoscalar and heavy Higgs boson masses depend on both  $\delta_{H_u}$  and  $\delta_{H_d}$ .

Table 1: SUSY masses (in GeV) for the point  $m_0 = 360$  GeV,  $m_{1/2} = 500$  GeV,  $\tan\beta = 40$ ,  $A_0 = 0$ , and  $m_H = 732$  GeV. For this point, the dark matter relic density is  $\Omega_{\tilde{\chi}_1^0} h^2 = 0.11$ . The total production cross-section for this point is  $\sigma = 1.25$  pb.

$\tilde{g}$	$\tilde{u}_L$	$\tilde{t}_2$	$\tilde{b}_2$	$\tilde{e}_L$	$\tilde{\tau}_2$	$\tilde{\chi}_2^0$	$\tilde{\chi}_4^0$	$\tilde{\chi}_2^\pm$
	$\tilde{u}_R$	$\tilde{t}_1$	$\tilde{b}_1$	$\tilde{e}_R$	$\tilde{\tau}_1$	$\tilde{\chi}_1^0$	$\tilde{\chi}_3^0$	$\tilde{\chi}_1^\pm$
1161	1113	992	989	494	446	293	432	427
	1078	781	946	407	255	199	316	291

In this model, the dark matter content can be satisfied not only by lowering  $\mu$  but also having the pseudoscalar or heavy Higgs mass equal to twice the neutralino mass. Since we have two new parameters in the Higgs sector, both the pseudoscalar mass and  $\mu$  are free parameters in this model. In the case where the dark matter content is satisfied by the heavy Higgs/pseudoscalar Higgs resonance, the heavy Higgs mass needs to be measured to see whether its mass obeys the resonant funnel condition. In our case we do not consider the Higgs funnel region but consider the first scenario where  $\mu$  is changed to satisfy the dark matter content. For the purposes of this study, we choose one such model which predicted a dark matter relic density in agreement with that measured by WMAP. This scenario is also very interesting since it has large direct detection spin-independent cross-section of  $3.56 \times 10^{-8}$  pb for proton collisions, and therefore it will be detected in the ongoing/upcoming runs of direct detection experiments [17].

Since  $\mu$  is affected by only the up type Higgs, we define the nuSUGRA model with the unified Higgs mass at the GUT scale,  $m_{H_u} = m_{H_d} \equiv m_H$ , which becomes the fifth parameter of the model. The mass spectrum for our benchmark point of the nuSUGRA model is shown in Table 1. We determine the mass spectrum for this model using ISASUGRA [18].

### 3 Characteristic Signal and Observables at the LHC

Our benchmark point of the nuSUGRA model shows some features which we observed in previous studies of mSUGRA scenarios [5, 6, 7, 8]. In particular, it still predicts that the LHC would see high  $p_T$  jets from squark decays to neutralinos and charginos, many  $\tau$ 's from neutralino and stau decays, and large missing transverse energy ( $\cancel{E}_T$ ) from the lightest neutralino escaping the detector. However, in this nuSUGRA region, we also see another unique final state: There are many  $W$  bosons being produced from neutralinos decaying into charginos or vice versa.

Since these  $W$  bosons seem to be a smoking gun signal, we perform a random parameter space scan in mSUGRA to see if  $W$  bosons are being produced or not. For values of  $\tan\beta = \{10, 40\}$ , we scan  $m_{1/2} < 1000$  GeV, and  $m_0 < 2000$  GeV, keeping  $A_0 = 0$  and  $\mu > 0$ . We also ensure that experimental bounds for the Higgs mass [19], lightest chargino mass [20], and squark masses [21] are not violated. The results of this scan show that  $W$  bosons in similar decay chains do appear in mSUGRA. However, under a thermal dark matter scenario, if we

constrain the relic density of the universe to be somewhat close to the WMAP allowed region (using  $\Omega_{\tilde{\chi}_1^0} h^2 < 0.3$ ), then we find that the only mSUGRA models with jet+ $2\tau$  and jet+ $W$  final states are in the co-annihilation region. This means that we can discern between mSUGRA and nuSUGRA at the LHC simply by measuring the difference in mass between the lightest stau and lightest neutralino (assuming a thermal dark matter scenario). For instance, in the coannihilation region of mSUGRA, the mass difference is  $\Delta M_{\tilde{\tau}_1 - \tilde{\chi}_1^0} = 5\text{-}20$  GeV, whereas in our nuSUGRA benchmark point  $\Delta M_{\tilde{\tau}_1 - \tilde{\chi}_1^0} = 56$  GeV.

Since this model can be discerned at the LHC, we study it to see if we can fully reconstruct the model. We use Monte Carlo programs which simulate a LHC experiment. To determine the mass spectrum of the model, we use ISASUGRA [18]. The mass spectrum is passed on to PYTHIA [22] to generate the Monte Carlo hard scattering events and hadron cascade. Unless otherwise specified, these events are 14 TeV  $pp$  collisions. Each such event is then passed on to PGS4 [23] to simulate the detector effects.

Since we require five independent measurements to determine our five model parameters, we construct as many useful measurements as possible. To this end, it is necessary to utilize the  $W$  boson decay chains. Reconstructing  $W$  bosons from their hadronic decays is difficult in a jets plus  $\cancel{E}_T$  final state. The leptonic decays of  $W$  decay are not adequate, since neutrinos, a source of  $\cancel{E}_T$ , are also produced. We instead reconstruct  $W$  bosons from their decays to quark pairs, i.e. jets in the detector. Thus, we must develop techniques of reconstructing  $W$  bosons from these jets.

There are several mass reconstruction techniques for finding new particles, such as classical endpoint measurements [24], mass relation techniques [25], and  $m_{T2}$  techniques [26]. We choose the endpoint measurements as the simplest technique with minimum assumptions in this study to demonstrate our proposed subtraction technique. We also assume that the SM background shapes are studied and subtracted in order to focus on this technique as well as the observables we use to fully determine the nuSUGRA parameters. The subtraction technique and LHC simulations of the observables are described in the following subsections

### 3.1 Bi-Event Subtraction Technique (BEST)

One such technique aims at an ability to select the particular jet pair originating from  $W$  boson decays. The difficulty is in discerning this jet pair from amongst the large combinatorial background of non- $W$  jets. We employ a subtraction technique to deal with this issue. This subtraction technique is similar to one used for a lepton plus jets system [27]. We collect all the jet pairs in an event, each of which could be (a) both from the  $W$  boson decay, (b) one from the  $W$  boson and one from another source, or (c) both from non- $W$  sources. These are “same-event” jet pairs with which we form the same-event dijet invariant mass distribution,  $M_{jj}^{\text{same}}$ .

If we know the shape of the distribution containing (b) and (c) jet pairs, we can subtract this distribution from  $M_{jj}^{\text{same}}$  to drastically reduce the background. To estimate the shape of this distribution, we collect all the jet pairs we can make by selecting one jet from the event of interest and one jet from a different event. We expect the “bi-event” dijet invariant mass distribution,  $M_{jj}^{\text{bi-event}}$ , to have a similar shape as most of the background in (b) and (c). Since

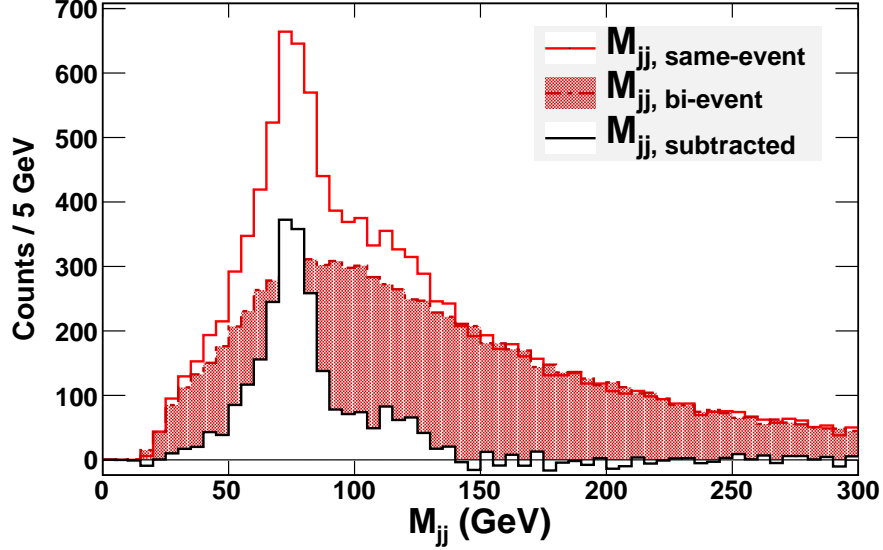


Figure 1: The di-jet invariant mass distribution for  $t\bar{t}$  in 7 TeV  $pp$  collisions with a luminosity of  $1 \text{ fb}^{-1}$ . This figure demonstrates our BEST for finding  $W$  bosons in the events. The solid red(grey) histogram is constructed using same-event jets. The dot-dashed and filled red(grey) histogram is constructed using jets from different (or bi-) events and is normalized to the shape of the long tail (above 200 GeV) in the same-event histogram. The same-event minus bi-event subtraction produces the black subtracted histogram. We notice a clear reduction in the background shape around the  $W$  mass peak.

there is no way for the bi-event jet pairs to come from a single  $W$  boson, it definitely does not match the shape of the (a) distribution. We normalize the  $M_{jj}^{\text{bi-event}}$  distribution to the  $M_{jj}^{\text{same}}$  distribution in the region of mass higher than the  $W$  boson. Then we subtract the  $M_{jj}^{\text{bi-event}}$  distribution from the  $M_{jj}^{\text{same}}$  distribution to get  $M_{jj}$ . This final  $M_{jj}$  distribution shows a nice  $W$  boson mass peak with a much smaller background than the original  $M_{jj}^{\text{same}}$  distribution. This “bi-event subtraction technique” is the BEST we can do for finding  $W$  bosons.

To demonstrate the BEST, we produced a small ( $1 \text{ fb}^{-1}$ )  $t\bar{t}$  sample of 7 TeV  $pp$  collisions. We selected events with the following cuts:

- Missing transverse energy,  $\cancel{E}_T \geq 25 \text{ GeV}$ ;
- Number of jets,  $N_{\text{jet}} \geq 4$  with jet  $p_T \geq 25 \text{ GeV}$  and  $|\eta| \leq 2.5$ ;
- At least one of the four jets must be  $b$  tagged;
- Exactly one lepton ( $e$  or  $\mu$  with  $p_T > 20 \text{ GeV}$ ).

With these events, we find the  $W$  mass peak without the top mass constraint in a  $j\bar{j}b$  final state. We select jet pairs with  $\Delta R_{jj} \geq 0.4$ , since jets which are too close cannot be discerned by the detector. The BEST  $W$  finding for this sample is shown in Fig. 1.

This technique helps us remove backgrounds from other signals as well. For instance, we often combine the two leading jets in each event (which come from the squark decays) with other

reconstructed objects to form an observable. Doing our BEST helps us to choose the correct jet from the decay chain we want. We perform our BEST in almost all of the observables described below.

### 3.2 $W$ Plus Jet

The  $W$  plus jet signal originates primarily from the following two decay chains:

$$\tilde{q} \rightarrow q + \tilde{\chi}_1^\pm \rightarrow q + W^\pm + \tilde{\chi}_1^0 \quad (2a)$$

$$\tilde{q} \rightarrow q + \tilde{\chi}_4^0 \rightarrow q + W^\pm + \tilde{\chi}_1^\mp \rightarrow \dots \quad (2b)$$

The signal is characterized by a high  $p_T$  jet and high  $\cancel{E}_T$  as well as a  $W$  boson, which we see in the detector as two jets with invariant mass in the  $W$  mass window ( $65 \text{ GeV} \leq m_{jj} \leq 90 \text{ GeV}$ ). We reconstruct the  $W$  boson and combine it with the corresponding leading  $p_T$  jet from this decay chain to make the  $W$  plus jet invariant mass,  $M_{jW}$ .

To select events for this signal, we use the following cuts:

- Missing transverse energy,  $\cancel{E}_T \geq 180 \text{ GeV}$ ;
- Number of jets,  $N_{\text{jet}} \geq 4$  with jet  $p_T \geq 30 \text{ GeV}$  and  $|\eta| \leq 2.5$ . (Here we do not count  $b$  tagged jets);
- The two leading jets must have  $p_T \geq 100 \text{ GeV}$ ;
- No leptons at all in the event (no  $\tau$  with  $p_T > 20 \text{ GeV}$ , and no  $e$  or  $\mu$  with  $p_T > 5 \text{ GeV}$ );
- The scalar sum,  $p_{T\text{jet},1} + p_{T\text{jet},2} + \cancel{E}_T \geq 600 \text{ GeV}$ ;
- There must be no  $b$  tagged jet with  $p_T$  larger than either of the two leading jets.

After the cuts are performed, we begin to pair up all of the jets (except for the two leading jets) to look for  $W$  candidates. The  $W$  bosons which are produced by the decay chain in Eq. 2 can have large momentum from being near the bottom of the cascade decay. Thus, we expect the jets pairs from the  $W$  to be close together due to Lorentz boosting. Again, the detector cannot discern the two jets if they are too close together. Therefore, we choose jet pairs which have  $0.4 \leq \Delta R_{jj} \leq 1.5$ . We have used a similar cut in our previous studies [8].

We sort our jet pairs into two categories: Those that are in the  $W$  mass window (where  $65 \text{ GeV} \leq m_{jj} \leq 90 \text{ GeV}$ ), and those that are clearly not  $W$ 's which are in the sideband window (where  $40 \text{ GeV} \leq m_{jj} \leq 55 \text{ GeV}$  or  $100 \text{ GeV} \leq m_{jj} \leq 115 \text{ GeV}$ ). We sort them this way for an upcoming sideband subtraction.

To help us find a clean  $W$  peak with not too much background in the way, we also perform our BEST. To this end, we combine each jet considered with a jet from the previous event. Again, we sort these bi-event jet pairs into the  $W$  mass window and the sideband window. We normalize the shape of the overall bi-event histogram by matching its tail with that of the same-event histogram and subtract. We are left with a  $W$  peak surrounded by much less background. To subtract off the remaining background, we perform the sideband subtraction.



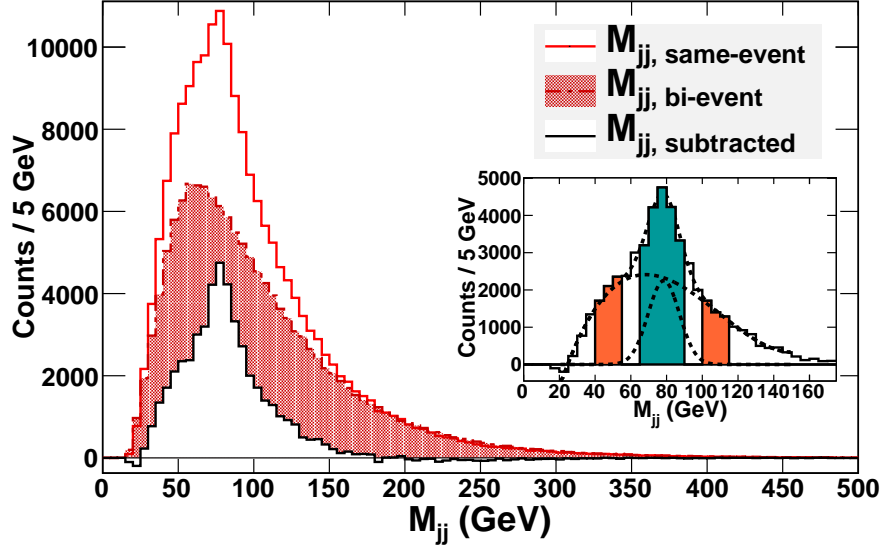


Figure 2: The di-jet invariant mass distribution for our benchmark point. This figure demonstrates our BEST as well as how we find  $W$  bosons in the events. The solid red(grey) histogram is constructed using same-event jets. The dot-dashed and filled red(grey) histogram is constructed using jets from different (or bi-) events and is normalized to the shape of the long tail in the same-event histogram. The same-event minus bi-event subtraction produces the black subtracted histogram. This subtracted histogram is plotted again in the inset plot. Also in the inset plot is shown the  $W$  mass window (which is the cyan filled region between 65 and 90 GeV), the sideband windows (which are the orange filled regions between 40 and 55 GeV as well as between 100 and 115 GeV), and the cubic plus Gaussian fit which describes the background and  $W$  peak shapes (shown as short dashed lines).

We demonstrate this  $W$  finding process, including our BEST and the sorting of jet pairs into the  $W$  mass and sideband windows, in Fig. 2.

Once we implement this method of finding and reconstructing  $W$  bosons, we begin to pair them up with leading jets. Once again, we perform our BEST to help us choose the correct leading jet (coming from the correct “side” of the collision event). So, we calculate the invariant mass  $M_{jW}$  for our  $W$  with leading jets from the same event, and again with leading jets from a different event. As before, we normalize the tail of the bi-event distribution to the shape of the tail of the same-event distribution and subtract. The final result is that the  $M_{jW}$  distribution shows a nice endpoint which can be fit with a simple line. A sample  $M_{jW}$  distribution which shows our BEST is shown in Fig. 3.

### 3.3 The $M_{\text{eff}}$ observable

The effective mass observable [24],  $M_{\text{eff}}$ , is a simple measure of the overall SUSY mass scale for many SUSY models. The signal is characterized by production of gluinos and squarks in the initial hard scattering events. The cascade decays of gluinos and squarks produce high

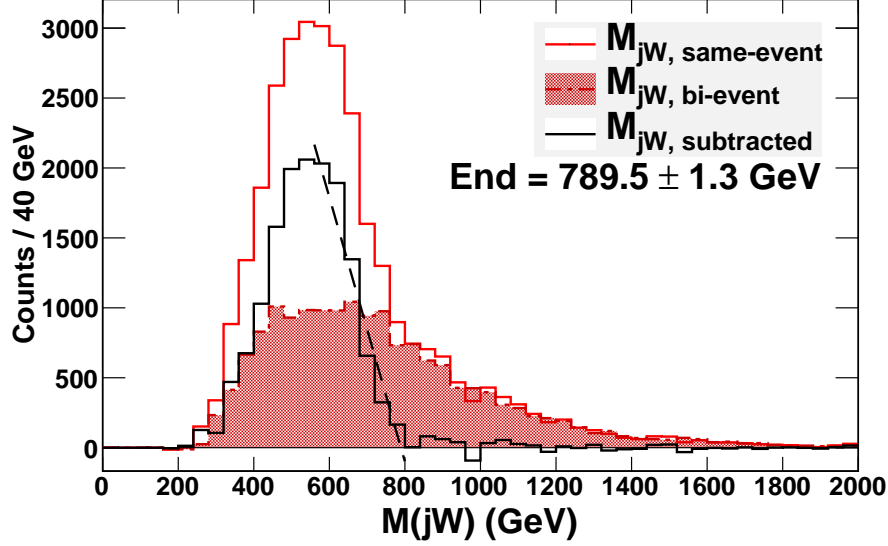


Figure 3: The jet +  $W$  invariant mass distribution for our benchmark point. This figure again demonstrates our BEST. The solid red(grey) histogram is constructed by combining each  $W$  with each of the two leading jets from the same event. The dot-dashed and filled red(grey) bi-event histogram is constructed by combining each  $W$  with each of the two leading jets from a different event and is normalized to the shape of the long tail in the same-event histogram. The same-event minus bi-event subtraction produces the black subtracted histogram. This subtracted histogram is then fitted with a straight line (shown as a dashed line in the figure) to find the endpoint of the distribution. The reported uncertainty in the figure is for an integrated luminosity of  $\mathcal{L} = 1000 \text{ fb}^{-1}$ .

transverse momentum jets and missing energy. The  $M_{\text{eff}}$  variable is defined as,

$$M_{\text{eff}} = p_{T\text{jet},1} + p_{T\text{jet},2} + p_{T\text{jet},3} + p_{T\text{jet},4} + \cancel{E}_T, \quad (3)$$

using the four highest transverse momentum ( $p_T$ ) jets of the event. Because we select the leading four jets, we effectively get the jets which originate from gluino and squark decays.

We select events for the  $M_{\text{eff}}$  observable with the following cuts [24]:

- Number of jets,  $N_{\text{jet}} \geq 4$  with jet  $p_T \geq 50 \text{ GeV}$  and  $|\eta| \leq 2.5$ ;
- None of the above jets can be  $b$  tagged;
- Highest jet  $p_{T\text{jet},1} \geq 100 \text{ GeV}$ ;
- No isolated  $\mu$  leptons or electrons in the event;
- Missing transverse energy,  $\cancel{E}_T \geq 200 \text{ GeV}$  and  $\cancel{E}_T \geq 0.2 * M_{\text{eff}}$ ;
- Transverse sphericity,  $S_T \leq 0.2$ .

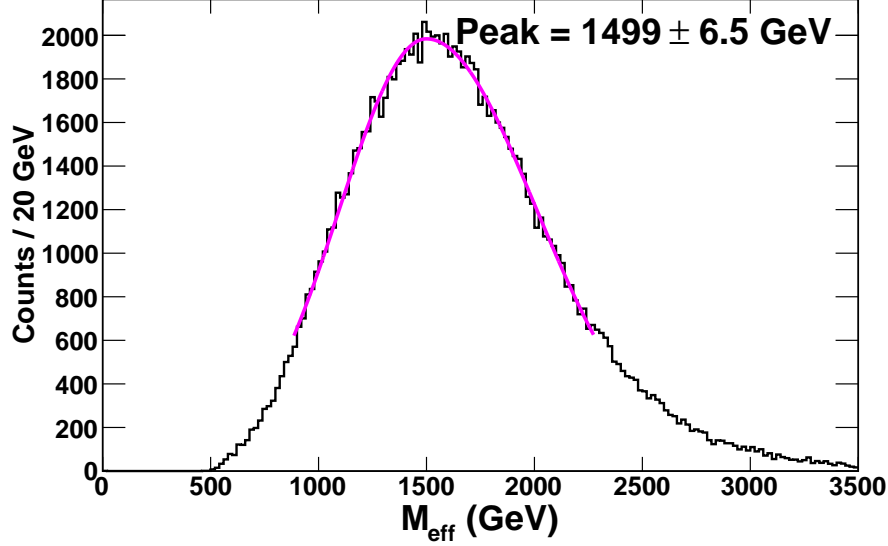


Figure 4: The effective mass distribution for our benchmark point. The curve through the histogram is the result of fitting with the asymmetric Gaussian function given by Eq. 4. The reported uncertainty in the figure is for an integrated luminosity of  $\mathcal{L} = 1000 \text{ fb}^{-1}$ .

Once events are selected in this way, the  $M_{\text{eff}}$  distribution is fit with an asymmetric Gaussian function:

$$N = \begin{cases} Ae^{-\frac{M_{\text{eff}} - M_{\text{eff}}^{\text{peak}}}{2\sigma_{\text{low}}^2}}, & \text{if } M_{\text{eff}} < M_{\text{eff}}^{\text{peak}} \\ Ae^{-\frac{M_{\text{eff}} - M_{\text{eff}}^{\text{peak}}}{2\sigma_{\text{high}}^2}}, & \text{if } M_{\text{eff}} \geq M_{\text{eff}}^{\text{peak}} \end{cases}, \quad (4)$$

where  $A$  is some constant scaling factor,  $M_{\text{eff}}^{\text{peak}}$  is the peak position, and  $\sigma_{\text{low}}$  and  $\sigma_{\text{high}}$  are the variances below and above the peak position, respectively. The most important result of the fit is the value of  $M_{\text{eff}}^{\text{peak}}$ . A sample  $M_{\text{eff}}$  distribution is shown in Fig. 4.

Another similar observable we define is  $M_{\text{eff}}^{(b, \text{ no } W)}$ . This observable also measures the SUSY scale, but includes information from third generation squarks. It is defined as,

$$M_{\text{eff}}^{(b, \text{ no } W)} = p_{Tb \text{ jet},1} + p_{T\text{jet},2} + p_{T\text{jet},3} + p_{T\text{jet},4} + \cancel{E}_T, \quad (5)$$

where in this case the leading jet (and only the leading jet) must be  $b$  tagged. The selection cuts we use for this observable are identical to those of  $M_{\text{eff}}$  with the exception that no pair of jets in the entire event can have an invariant mass in the  $W$  boson mass window. We define this mass window to be between 65 and 90 GeV. The  $M_{\text{eff}}^{(b, \text{ no } W)}$  distribution is fit in the same way as  $M_{\text{eff}}$ . The plot of this distribution looks very similar in shape with the  $M_{\text{eff}}$  distribution shown in Fig. 4.

### 3.4 Jet Plus $2\tau$

The jet plus  $2\tau$  signal originates from the following two decay chains:

$$\tilde{q} \rightarrow q + \tilde{\chi}_2^0(\tilde{\chi}_3^0) \rightarrow q + \tau^\mp + \tilde{\tau}_1^\pm \rightarrow q + \tau^\mp + \tau^\pm + \tilde{\chi}_1^0 \quad (6)$$

The signal is characterized by a high  $p_T$  jet and high  $\cancel{E}_T$  as well as a pair of oppositely charged  $\tau$  leptons.

We used the following cuts [5, 6, 7] to select events for this signal:

- Missing transverse energy,  $\cancel{E}_T \geq 180$  GeV;
- At least two jets with jet  $p_T \geq 200$  GeV and  $|\eta| \leq 2.5$  (here we do not count  $b$  tagged jets);
- No  $\mu$ 's or electrons at all in the event;
- At least two identified  $\tau$  leptons [23] in the event with  $\tau$   $p_T \geq 20$  GeV and  $|\eta| \leq 2.5$ ;
- The scalar sum,  $p_{T\text{jet},1} + p_{T\text{jet},2} + \cancel{E}_T \geq 600$  GeV;
- There must be no  $b$  tagged jet with  $p_T$  larger than either of the two leading jets.

This signal can be utilized to make three independent observables,  $M_{\tau\tau}$ ,  $M_{j\tau\tau}$ , and  $M_{j\tau}$ .

#### 3.4.1 $M_{\tau\tau}$

To construct this observable we only need to combine  $\tau$  pairs from each event. We sort the  $\tau$  pairs into similarly charged or “like-sign” (LS) pairs as well as oppositely charged or “opposite-sign” (OS) pairs. The OS pairs contain  $\tau$  pairs from our desired decay chain as well as random  $\tau$  pairs, whereas the LS pairs contain only random  $\tau$  pairs. Thus, we perform an OS–LS subtraction to make the  $2\tau$  invariant mass,  $M_{\tau\tau}$ . This distribution shows a nice endpoint which can be determined by fitting with a simple line. A sample distribution showing the OS–LS subtraction is shown in Fig. 5. Due to the inability to fully reconstruct each  $\tau$  (because of neutrinos which are missing energy), a small shoulder appears in the figure beyond the endpoint. However, this shoulder is not in the way of finding the endpoint for this case.

#### 3.4.2 $M_{j\tau\tau}$

As for  $M_{\tau\tau}$ , we consider all  $\tau$  pairs from each event, sorting them into OS and LS pairs. We combine each pair with each of the leading jets to fill the same-event jet plus  $2\tau$  invariant mass distribution,  $M_{j\tau\tau}^{\text{same}}$ . Additionally, each  $\tau$  pair is combined with each of the two leading jets from a different event to fill the bi-event distribution,  $M_{j\tau\tau}^{\text{bi-event}}$ . The OS–LS subtraction is performed first, followed by our BEST. As before, the bi-event histogram is normalized to the shape of the tail in the same-event histogram prior to the subtraction. The result of this process is the  $M_{j\tau\tau}$  distribution. Unlike our  $M_{\tau\tau}$  observable, we do not see a sharp endpoint. Due to the effects of missing energy from each  $\tau$  (when the neutrino escapes the detector) as well as combining those  $\tau$ 's with a jet, the endpoint gets washed out. Instead, we choose the peak position for our  $M_{j\tau\tau}$  observable. This peak is found by fitting with either a regular Gaussian or asymmetric Gaussian (seen in Eq. 4), depending on the shape of the distribution. A sample distribution showing our BEST is shown in Fig. 6.

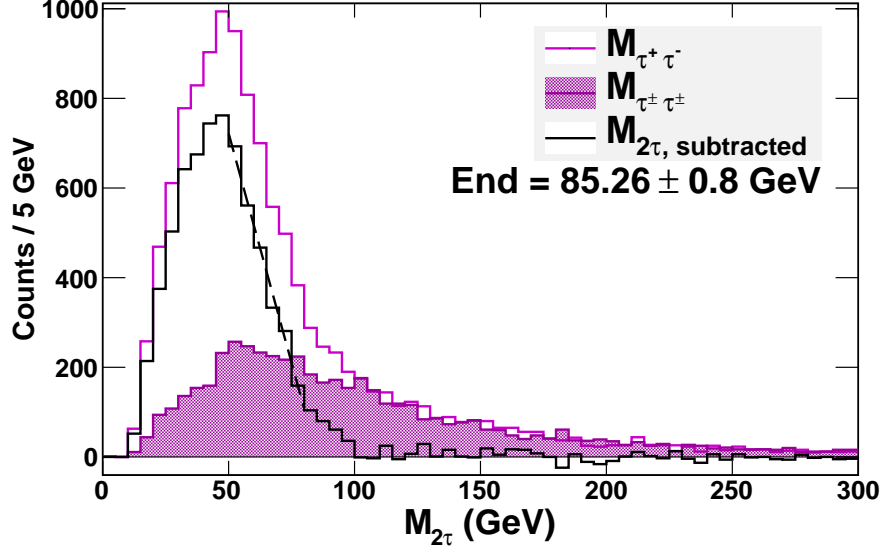


Figure 5: The  $2\tau$  invariant mass distribution for our benchmark point. The solid magenta(grey) histogram is composed of OS  $\tau$  pairs, while the dot-dashed and filled magenta(grey) histogram is composed of LS  $\tau$  pairs. The OS–LS subtraction produces the black subtracted histogram. This subtracted histogram is then fitted with a straight line (shown as a dashed line in the figure) to find the endpoint of the distribution. The reported uncertainty in the figure is for an integrated luminosity of  $\mathcal{L} = 1000 \text{ fb}^{-1}$ .

### 3.4.3 $M_{j\tau}$

To construct this observable we consider  $\tau$  pairs in the event and combine one of the  $\tau$ 's with the corresponding leading jets. There is an ambiguity which arises due to the choice of which  $\tau$  to use in the observable. The way we deal with this ambiguity is described below.

Similarly as before we collect all possible  $\tau$  pairs in the event, sorting them into OS and LS pairs. For each leading jet, the invariant mass,  $M_{j\tau}$ , is determined for each tau. These two values are compared, and stored in two histograms. The histograms are labeled as  $M_{j\tau}^{(1st)}$ , which contains the larger of the two  $M_{j\tau}$  values for each jet, and  $M_{j\tau}^{(2nd)}$ , which contains the smaller. A similar procedure is performed for the two leading jets from a different event to form bi-event distributions. The OS–LS subtraction is performed, followed by our BEST. This leaves us with two resulting final distributions of  $M_{j\tau}^{(1st)}$  and  $M_{j\tau}^{(2nd)}$ .

For this region of parameter space, there is a systematic way to choose between these histograms to find an endpoint which is close in agreement with the theoretical prediction. By default, the  $M_{j\tau}^{(1st)}$  histogram is chosen and fit with a line to find the endpoint of the distribution. However, if the behavior of the endpoint region does not seem linear, we choose  $M_{j\tau}^{(2nd)}$ . We also make this choice if the BEST does not appear to work. The BEST can fail if there are not enough signal events compared to background events. If the BEST fails like this for  $M_{j\tau}^{(1st)}$ , it tells us we are not picking up the decay chain we want to look at, so we choose  $M_{j\tau}^{(2nd)}$  instead. A sample distribution for our benchmark point is shown in Fig. 7. Since we have less missing energy here (only one  $\tau$ ), we can see the endpoint clearly for this observable.

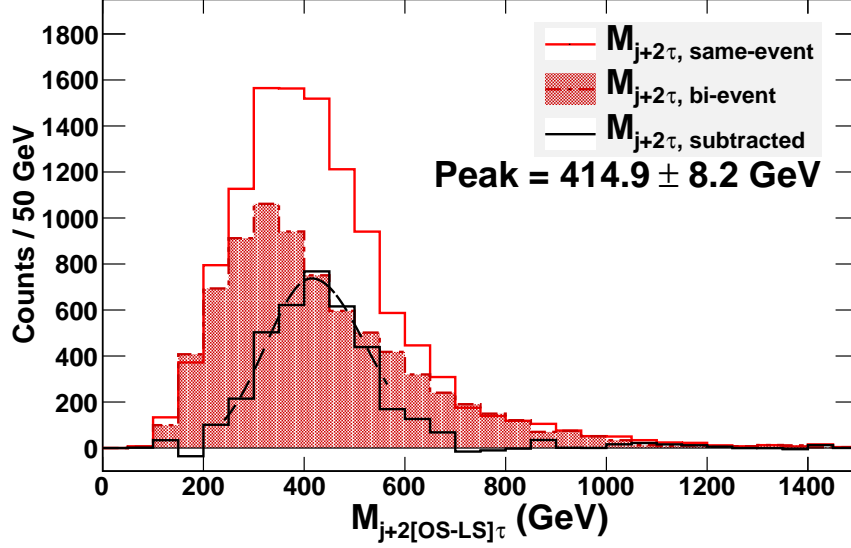


Figure 6: The jet +  $2\tau$  invariant mass distribution for our benchmark point. This figure again demonstrates our BEST. The solid red(grey) histogram is constructed by combining each OS–LS  $\tau$  pair with each of the two leading jets from the same event. The dot-dashed and filled red(grey) bi-event histogram is constructed by combining each OS–LS  $\tau$  pair with each of the two leading jets from a different event and is normalized to the shape of the long tail in the same-event histogram. The same-event minus bi-event subtraction produces the black subtracted histogram. This subtracted histogram is then fitted with a Gaussian function (shown as a dashed curve in the figure) to find the peak of the distribution. The reported uncertainty in the figure is for an integrated luminosity of  $\mathcal{L} = 1000 \text{ fb}^{-1}$ .

## 4 Determining Model Parameters and Relic Density

With the six observables in section 3, we determine the model parameters. We vary each model parameter independently about our benchmark point to find how each observable behaves as a function of the model parameters. We simulate the LHC experiment for each point, and determine all the observables along with their uncertainties. For each observable, we plot the value of the observable as a function of each model parameter. Fits through these plots determine the “functional form” for our observables in a similar fashion as in Ref. [7].

In this region of nuSUGRA parameter space, the observables behave in a fortunate manner. Some observables are only functions of some of the model parameters, while being constant with respect to variations in other model parameters. The functional forms are as follows:

- $M_{\text{eff}}^{\text{peak}} = f_1(m_{1/2})$ ;
- $M_{\text{eff}}^{(b, \text{no } W) \text{ peak}} = f_2(m_{1/2})$ ;
- $M_{jW}^{\text{end}} = f_3(m_{1/2}, m_H)$ ;
- $M_{j\tau\tau}^{\text{peak}} = f_4(m_{1/2}, m_H, m_0)$ ;

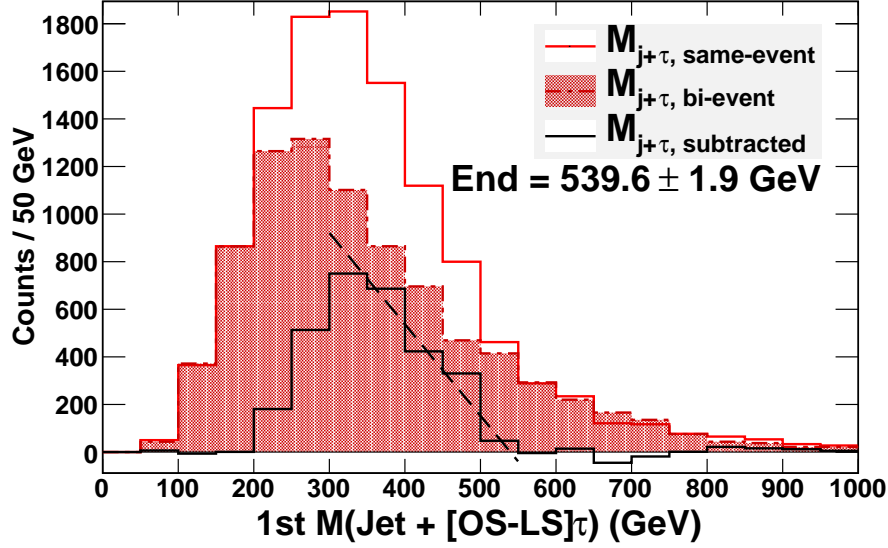


Figure 7: The jet +  $\tau$  invariant mass distribution for our benchmark point. This figure again demonstrates our BEST. The solid red(grey) histogram is constructed by combining each OS–LS  $\tau$  with each of the two leading jets from the same event, choosing the  $\tau$  which gives the larger value of  $M_{j\tau}$ . The dot-dashed and filled red(grey) bi-event histogram is constructed the same way with each of the two leading jets from a different event and is normalized to the shape of the long tail in the same-event histogram. The same-event minus bi-event subtraction produces the black subtracted histogram. This subtracted histogram is then fitted with a linear function (shown as a dashed line in the figure) to find the endpoint of the distribution. The reported uncertainty in the figure is for an integrated luminosity of  $\mathcal{L} = 1000 \text{ fb}^{-1}$ .

- $M_{\tau\tau}^{\text{end}} = f_5(m_{1/2}, m_H, m_0, A_0);$
- $M_{j\tau}^{\text{end}} = f_6(m_{1/2}, m_H, m_0, A_0, \tan \beta).$

These functional forms are found by varying one parameter at a time to see how the observables change. However, they make a lot of sense. The sensitivity of each observable on a model parameter depends on the relative change that varying that parameter will affect the observable. For instance, the  $M_{\text{eff}}$  observables have peak values that are quite large ( $\simeq 1500 \text{ GeV}$ ), so small changes in the squark masses (caused by varying  $m_0$ ,  $A_0$ , or  $\tan \beta$ ) are undetected. Thus, in this region of parameter space, the  $M_{\text{eff}}$  observables are only a function of  $m_{1/2}$ . A similar effect happens for  $M_{jW}$  as well. However,  $M_{jW}$  also depends on neutralino and chargino masses which are strongly affected by  $\mu(m_H)$ . Both squark masses and neutralino masses show a slight  $m_0$  dependence. Since, for  $M_{j\tau\tau}$ , we are looking at the relatively small peak position ( $\simeq 400 \text{ GeV}$ ), we pick up this  $m_0$  sensitivity. Lastly, the  $M_{\tau\tau}$  and  $M_{j\tau}$  feel the involvement of the stau particle, showing dependencies on  $m_0$ ,  $A_0$ , and  $\tan \beta$ .

This behavior allows us to solve for one parameter at a time. The result of each model parameter is used as input for the next parameter to be solved for. In this manner, solving for each parameter is as simple as solving for one unknown from one equation. However, the uncertainty in each solved parameter would then influence the next one to be solved for.

Table 2: Results of the nuSUGRA model parameters and relic density of dark matter in the universe for integrated luminosities of  $\mathcal{L} = 1000 \text{ fb}^{-1}$  and  $\mathcal{L} = 100 \text{ fb}^{-1}$  [29]. Note that the uncertainties for an integrated luminosity of  $\mathcal{L} = 100 \text{ fb}^{-1}$  were estimated by simply scaling down the distributions before performing fits for the analysis.

$\mathcal{L} \text{ (fb}^{-1}\text{)}$	$m_{1/2} \text{ (GeV)}$	$m_H \text{ (GeV)}$	$m_0 \text{ (GeV)}$	$A_0 \text{ (GeV)}$	$\tan \beta$	$\mu \text{ (GeV)}$	$\Omega_{\tilde{\chi}_1^0} h^2$
1000	$499.5 \pm 3.2$	$727 \pm 10$	$366 \pm 26$	$3 \pm 34$	$39.5 \pm 3.8$	$321 \pm 25$	$0.094^{+0.107}_{-0.038}$
100	$499.6 \pm 9.3$	$727 \pm 13$	$367 \pm 57$	$0 \pm 73$	$39.5 \pm 4.6$	$331 \pm 48$	$0.088^{+0.168}_{-0.072}$

To estimate this effect, we use the uncertainty in each parameter as an additional source of uncertainty for the next observable. All such uncertainties are estimated using simple Monte Carlo programs.

To illustrate this whole process, we describe the first few logical steps in how we determine the model parameters:  $M_{\text{eff}}^{\text{peak}}$  and  $M_{\text{eff}}^{(b, \text{no } W) \text{ peak}}$  are only functions of  $m_{1/2}$ , so we use each to solve for  $m_{1/2}$  separately, then combine the measurements. This measurement combination reduces the uncertainty slightly (around a 7% uncertainty reduction) as compared to using  $M_{\text{eff}}^{\text{peak}}$  alone. Next, we propagate the uncertainty in  $m_{1/2}$  to an additional uncertainty in  $M_{jW}^{\text{end}}$  by using the  $M_{jW}^{\text{end}}$  versus  $m_{1/2}$  functional form. This uncertainty is added in quadrature to the measurement uncertainty in  $M_{jW}^{\text{end}}$ . With the uncertainty in  $M_{jW}^{\text{end}}$  estimated this way, we use the  $M_{jW}^{\text{end}}$  versus  $m_H$  functional form to solve for  $m_H$ . Then the uncertainties in  $m_{1/2}$  and  $m_H$  are propagated as additional uncertainties in  $M_{j\tau\tau}^{\text{peak}}$  while solving for  $m_0$ . The process continues like this all the way down the above list of functional forms.

Once we have finally determined all the model parameters, we use **darkSUSY** [28] to calculate the dark matter relic density of the universe today,  $\Omega_{\tilde{\chi}_1^0} h^2$ . We also estimate the uncertainty in the dark matter relic density due to the uncertainties in the measured model parameters. Our results are shown in Table 2. We find that the model parameters  $m_0$ ,  $m_{1/2}$ ,  $m_H$  and  $\tan \beta$  can be determined with less than 10% accuracy for  $100 \text{ fb}^{-1}$  luminosity. We can determine the accuracy of  $\mu$  from these parameters and we find that  $\mu$  can be determined with accuracies of around 15% and 8% for luminosities of  $100 \text{ fb}^{-1}$  and  $1000 \text{ fb}^{-1}$ , respectively.

Since the dark matter content is sensitive to the value of  $\mu$ , in Fig. 8, we plot one  $\sigma$  contours of the dark matter content as a function of  $\mu$  for luminosities of  $100 \text{ fb}^{-1}$  (red shaded region) and  $1000 \text{ fb}^{-1}$  (brick shaded region). The determination of dark matter content is of course much better with  $1000 \text{ fb}^{-1}$ , but even with  $100 \text{ fb}^{-1}$  the measurement accuracy is quite encouraging.

## 5 Conclusions and Discussion

In this paper we have shown that the LHC has an ability to investigate the origin of dark matter by establishing SUSY models. At the LHC, the colored SUSY particles, the squarks and gluinos, will be produced profusely. The squarks and gluinos will then go through cascade



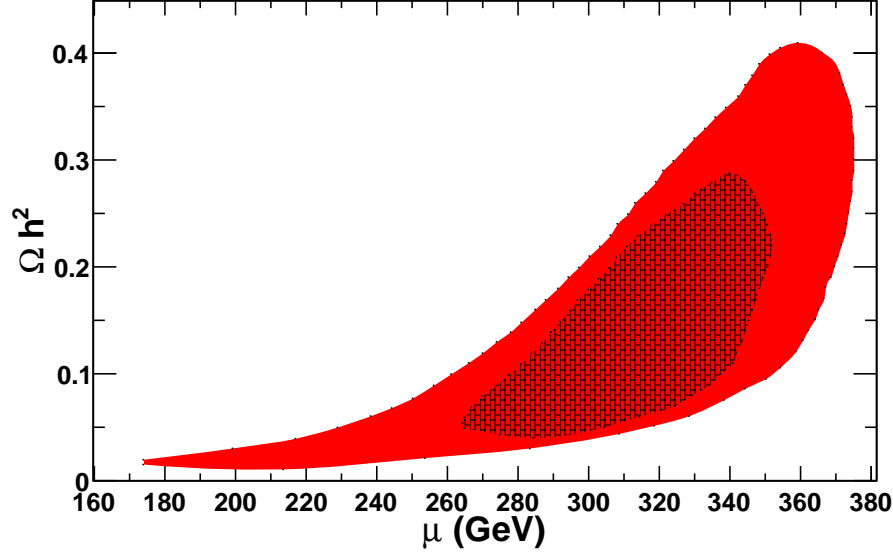


Figure 8: Estimates of  $1\sigma$  uncertainties in the  $\Omega_{\tilde{\chi}_1^0} h^2$  versus  $\mu$  plane. The solid red (brick textured) region is for a luminosity of  $\mathcal{L} = 100 \text{ fb}^{-1}$  ( $\mathcal{L} = 1000 \text{ fb}^{-1}$ ).

decays into final states involving the SM particles and missing energy. The challenge is to reconstruct masses or model parameters by forming observables using these final states. If we can reconstruct the model we will be able to calculate the dark matter content and check whether the established model explains the cosmology correctly. In this way, establishing the MSSM could be very hard. We may not have enough observables to measure all the parameters of the MSSM. Also not all the particles of the model would show up in the cascade decays with sufficient branching ratios. We therefore started with a simpler model where the gaugino masses are unified, and all scalar masses except that of the Higgs bosons are also unified at the GUT scale. This type of model is quite realistic and very popular since the explanation of dark matter becomes easy. The explanation can occur either via a large Higgsino component in the neutralino or via a resonance with the heavy or pseudoscalar Higgs. Here we considered the scenario with the larger Higgsino component. This scenario also gives rise to a larger direct detection cross-section and therefore can be detected in the upcoming direct detection experimental results.

Since SUSY production occurs in pairs of colored SUSY particles, each event has two decay chains. The particle from one decay chain will create background for any measurement of mass involving the other decay chain. In this paper, we first established techniques to remove this kind of background by combining particles from different events. We then created observables to establish the model. In previous works, when we tried to establish the mSUGRA model, we found that the observables mostly involved leptons, jets, Higgs bosons and  $Z$  bosons. However, for this nonuniversal Higgs model, nuSUGRA, we found that the final states involved  $W$  bosons arising from chargino decays in addition to jets, and  $\tau$  leptons in the final states. We constructed observables, e.g.,  $Wj$ ,  $j\tau\tau$ ,  $\tau\tau$  etc. and use them to determine masses and the model parameters. We showed that the model parameters can be determined with good accuracy (e.g.  $m_0$ ,  $m_{1/2}$ ,  $m_H$ , and  $\tan\beta$  can be determined with less than 10% accuracy) at a luminosity of  $\mathcal{L} = 100 \text{ fb}^{-1}$ .

The parameter  $\mu$  can be determined with an accuracy of 15% for the same luminosity. Finally, we showed that the dark matter content also can be determined in agreement with the WMAP experiment.

## Acknowledgments

This work is supported in part by the DOE grant DE-FG02-95ER40917 and by the World Class University (WCU) project through the National Research Foundation (NRF) of Korea funded by the Ministry of Education, Science & Technology (grant No. R32-2008-000-20001-0). We would like to thank A. Gurrola and Y. Santoso for useful discussions.

## References

- [1] WMAP Collaboration, D.N. Spergel *et al.*, *Astrophys. J. Suppl.* **148** (2003) 175.
- [2] H. Goldberg, *Phys. Rev. Lett.* **50** (1983) 1419; J. Ellis, J. Hagelin, D. Nanopoulos, K. Olive, and M. Srednicki, *Nucl. Phys. B* **238** (1984) 453.
- [3] D. Z. Freedman, P. Van Nieuwenhuisen, and S. Ferrara, *Phys. Rev. D* **13** (1976) 3214; S. Deser and B. Zumino, *Phys. Lett. B* **65** (1976) 369; A.H. Chamseddine, R. Arnowitt, and P. Nath, *Phys. Rev. Lett.* **49** (1982) 970; R. Barbieri, S. Ferrara, and C.A. Savoy, *Phys. Lett. B* **119** (1982) 343; L. Hall, J. Lykken, and S. Weinberg, *Phys. Rev. D* **27** (1983) 2359; P. Nath, R. Arnowitt, and A.H. Chamseddine, *Nucl. Phys. B* **227** (1983) 121; For a review, see P. Nilles, *Phys. Rep.* **100** (1984) 1.
- [4] M. Alam *et al.*, *Phys. Rev. Lett.* **74** (1995) 2885.
- [5] R. Arnowitt *et al.*, *Phys. Lett. B* **639** (2006) 46.
- [6] R. Arnowitt *et al.*, *Phys. Lett. B* **649** (2007) 73.
- [7] R. Arnowitt *et al.*, *Phys. Rev. Lett.* **100** (2008) 231802.
- [8] B. Dutta *et al.*, *Phys. Rev. D* **79** (2009) 055002.
- [9] P. Nath and R. Arnowitt, *Phys. Rev.* **D56** (1997) 2820.
- [10] See for example:  
H. Baer *et al.*, *Phys. Rev. D* **71** (2005) 095008 and *JHEP* **0507** (2005) 065; J. R. Ellis, K. A. Olive, and Y. Santoso, *Phys. Lett. B* **539** (2002) 107 and *J. High Energy Phys.* **0810** (2008) 005; J. R. Ellis, T. Falk, K. A. Olive, and Y. Santoso, *Nucl. Phys. B* **652** (2003) 259; J. R. Ellis, K. A. Olive, and P. Sandick, *New J. Phys.* **11** (2009) 105015; J. R. Ellis, S. F. King, and J. P. Roberts, *J. High Energy Phys.* **0804** (2008) 099; A. Bottino, F. Donato, N. Fornengo, and S. Scopel, *Phys. Rev. D* **59** (1999) 095004 and *Phys. Rev. D* **63** (2001) 125003; E. Accomando, R. L. Arnowitt, B. Dutta, and Y. Santoso, *Nucl. Phys. B* **585** (2000) 124; S. Bhattacharya *et al.*, *Phys. Rev. D* **81** (2010) 075009; L. Roszkowski

- et al.*, hep-ph/0903.1279; U. Chattopadhyay and D. Das, Phys. Rev. D **79** (2009) 035007; A. De Roeck *et al.*, Eur. Phys. J. C **49** (2007) 1041; D. G. Cerdeno and C. Munoz, J. High Energy Phys. **0410** (2004) 015.
- [11] J. Ellis, K. Olive, Y. Santoso, and V. Spanos, Phys. Lett. B **565** (2003) 176; R. Arnowitt, B. Dutta, and B. Hu, hep-ph/0310103; H. Baer *et al.*, J. High Energy Phys. **0306** (2003) 054; A. B. Lahanas and D.V. Nanopoulos, Phys. Lett. B **568** (2003) 55; U. Chattopadhyay, A. Corsetti, and P. Nath, Phys. Rev. D **68** (2003) 035005; E. Baltz and P. Gondolo, J. High Energy Phys. **0410** (2004) 052; A. Djouadi, M. Drees, and J. L. Kneur, J. High Energy Phys. **0603** (2006) 033; G. Belanger, S. Kraml, and A. Pukhov, Phys. Rev. D **72** (2005) 015003.
  - [12] J. Ellis, T. Falk and K. Olive, Phys. Lett. B **444** (1998) 367; J. Ellis, T. Falk, K. Olive and M. Srednicki, Astropart. Phys. **13** (2000) 181; M.E. Gomez, G. Lazarides and C. Pallis, Phys. Rev. D **61** (2000) 123512 and Phys. Lett. B **487** (2000) 313; A. Lahanas, D. V. Nanopoulos and V. Spanos, Phys. Rev. D **62** (2000) 023515; R. Arnowitt, B. Dutta and Y. Santoso, Nucl. Phys. B **606** (2001) 59.
  - [13] C. Bohm, A. Djouadi and M. Drees, Phys. Rev. D **62** (2000) 035012; J. R. Ellis, K. A. Olive and Y. Santoso, Astropart. Phys. **18** (2003) 395; J. Edsjo *et al.*, JCAP 0304 (2003) 001.
  - [14] M. Drees and M. Nojiri, Phys. Rev. D **47** (1993) 376; H. Baer and M. Brhlik, Phys. Rev. D **57** (1998) 567; H. Baer, M. Brhlik, M. Diaz, J. Ferrandis, P. Mercadante, P. Quintana and X. Tata, Phys. Rev. D **63** (2001) 015007; J. Ellis, T. Falk, G. Ganis, K. Olive and M. Srednicki, Phys. Lett. B **510** (2001) 236; L. Roszkowski, R. Ruiz de Austri and T. Nihei, J. High Energy Phys. **0108** (2001) 024; A. Djouadi, M. Drees and J. L. Kneur, J. High Energy Phys. **0108** (2001) 055; A. Lahanas and V. Spanos, Eur. Phys. J. C **23** (2002) 185.
  - [15] R. Arnowitt and P. Nath, Phys. Rev. Lett. **70** (1993) 3696; H. Baer and M. Brhlik, Ref. [22]; A. Djouadi, M. Drees and J. Kneur, Phys. Lett. B **624** (2005) 60.
  - [16] K. L. Chan, U. Chattopadhyay and P. Nath, Phys. Rev. D **58** (1998) 096004; J. Feng, K. Matchev and T. Moroi, Phys. Rev. Lett. **84** (2000) 2322 and Phys. Rev. D **61** (2000) 075005; see also H. Baer, C. H. Chen, F. Paige and X. Tata, Phys. Rev. D **52** (1995) 2746 and Phys. Rev. D **53** (1996) 6241; H. Baer *et al.*, Phys. Rev. D **59** (1999) 055014.
  - [17] CDMS Collaboration, <http://cdms.berkeley.edu/>; XENON100 Collaboration, <http://xenon.physics.rice.edu/>; Edelweiss Collaboration, <http://edelweiss.in2p3.fr/>; LUX Collaboration, <http://lux.brown.edu/>.
  - [18] F. E. Paige *et al.*, [arXiv:hep-ph/0312045]. We use ISAJET version 7.74.
  - [19] ALEPH, DELPHI, L3, OPAL Collaborations, G. Abbiendi *et al.* (The LEP Working Group for Higgs Boson Searches), Phys. Lett. B **565** (2003) 61.
  - [20] Particle Data Group, S. Eidelman *et al.*, Phys. Lett. B **592** (2004) 1.

- [21] S. P. Das, A. Datta, and M. Maity, Phys. Lett. B **596** (2004) 293.
- [22] T. Sjostrand, S. Mrenna, and P. Skands, J. High Energy Phys. **0605** (2007) 026. We use PYTHIA version 6.411 with TAUOLA.
- [23] PGS4 is a parameterized detector simulator. We use version 4 (<http://www.physics.ucdavis.edu/~conway/research/software/pgs/pgs4-general.htm>) in the CMS detector configuration. We assume the  $\tau$  identification efficiency with  $p_T^{\text{vis}} > 20$  GeV is 50%, while the probability for a jet being mis-identified as a  $\tau$  is 1%. The  $b$ -jet tagging efficiency in PGS is  $\sim 42\%$  for  $E_T > 50$  GeV and  $|\eta| < 1.0$ , and degrading between  $1.0 < |\eta| < 1.5$ . The  $b$ -tagging fake rate for  $c$  and light quarks/gluons is  $\sim 9\%$  and  $2\%$ , respectively.
- [24] I. Hinchliffe *et al.*, Phys. Rev. D **55** (1997) 5520; I. Hinchliffe and F. E. Paige, Phys. Rev. D **61** (2000) 095011; H. Bachacou, Ian Hinchliffe, and Frank E. Paige Phys. Rev. D **62** (2000) 015009.
- [25] K. Kawagoe, M. M. Nojiri, and G. Polesellom Phys. Rev. D **71** (2005) 035008.
- [26] C. G. Lester and D.J. Summers, Phys. Lett. B **463** (1999) 99; W. S. Cho *et al.*, Phys. Rev. Lett. **100** (2008) 171801.
- [27] ATLAS Collaboration, N. Ozturk, [arXiv:hep-ph/0710.4546].
- [28] P. Gondolo *et al.*, [arXiv:astro-ph/0211238].
- [29] All uncertainties are statistical only. The systematic uncertainties will be evaluated correctly once the LHC turns on.